Journal of Porous Materials (2019) 26:247–259
https://doi.org/10.1007/s10934-018-0644-x

Preparation and characterization of PCL-coated porous hydroxyapatite scaffolds in the presence of MWCNTs and graphene for orthopedic applications

Aylin M. Deliormanlı[1] · Mert Türk[1] · Harika Atmaca[2]

Published online: 20 July 2018
© Springer Science+Business Media, LLC, part of Springer Nature 2018

Abstract
Macro-channeled porous hydroxyapatite (HA) scaffolds were fabricated by a polymer foam replication method. Composites were prepared by coating the surface of HA scaffolds with polycaprolactone (PCL) in the presence of graphene nanopowders (in the form of flakes) and multi-walled carbon nanotubes (MWCNTs) at different concentrations. Compression strength of the scaffolds was investigated as a function of additive concentration. Results revealed that the use of PCL coating increased the mechanical strength of HA scaffolds. Besides, addition of graphene or MWCNTs further improved the compression strength of the constructs when they were used at 0.25 wt% and a decrease was observed at higher graphene and MWCNT concentrations. Highest mechanical performance was obtained in composite HA scaffolds involving MWCNTs. In vitro acellular bioactivity experiments revealed that both graphene and MWCNT-incorporated HA scaffolds showed higher bioactivity in simulated body fluid compared to bare scaffolds. However, HA formation ability was more pronounced with MWCNTs compared to graphene nanoflakes where they were possibly acted as an effective nucleation sites to induce the formation of a biomimetic apatite. Additionally, scaffolds prepared in the study were found to be nontoxic to the mouse bone marrow mesenchymal stem cells.

Keywords Hydroxyapatite · Polycaprolactone · Graphene · MWCNTs · Tissue engineering

1 Introduction

Synthetic hydroxyapatite, ($Ca_{10}(PO_4)_6(OH)_2$) is a bioceramic material widely used in bone tissue engineering and dental applications due to its high biocompatibility and ability to bond hard tissues [1–4]. It is chemically and crystallographically similar to natural apatite found in bones [5]. It is able to guide and stimulate bone growth and forming a secure bond with the surrounding tissue [6, 7]. However, compression strength and fracture toughness of pure HA cannot match the mechanical properties of bone tissue and restrict its uses in major load-bearing applications [4, 6, 8, 9]. Therefore, the application of bulk HA for hard tissue implants are limited. Consolidated HA scaffolds having high porosity with randomly distributed macro-channeled pores generally possess a typical compressive strength below 10 MPa [6]. This value is far below the compression strength of compact bone [10]. To solve this problem, materials with higher mechanical performance are used as reinforcing agents to improve the mechanical properties of HA [4]. Alternatively, HA powders and scaffolds can be combined with natural and synthetic polymers such as polycaprolactone, polyglycolic acid and polylactic acid to increase their strength and reduce brittleness [2, 11, 12]. Besides the poor mechanical properties, hydroxyapatite powders are not electrically conducting materials and that may limit their applications where electrically stimulated growth of the cells is required.

On the other hand, carbon nanostructures have gained massive attention in recent years. Graphene is a single layer of sp^2 hybridised carbon atoms. Similarly, single-walled carbon nanotubes are an allotrope of sp^2 hybridized carbon [13]. Multi-walled carbon nanotubes (MWCNTs) consist of

✉ Aylin M. Deliormanlı
aylin.deliormanli@cbu.edu.tr;
aylin.deliormanli12@gmail.com

[1] Department of Metallurgical and Materials Engineering, Faculty of Engineering, Manisa Celal Bayar University, Yunusemre, Manisa, Turkey

[2] Department of Biology, Faculty of Science and Literature, Manisa Celal Bayar University, Yunusemre, Manisa, Turkey

multiple layers of graphite rolled in to form a tubular shape [14]. Both of these carbon-based nano-materials attracted special interest in the scientific community due to their high mechanical, electrical and thermal properties [15, 16]. They can be utilized in electronic devices and electrochemical sensors since their electrical conductivity and charge carrier mobility is higher than the most conductive polymers by several orders of magnitude [14, 15]. Both graphene and MWCNTs could also be applied as an excellent reinforcement to ceramic materials as well as to the polymers [16–19]. Recent studies have shown that they have also significant potential in biomedical applications such as drug delivery, cancer treatment, biological sensors, antibacterial agent and biocompatible scaffold manufacture [14, 20].

CNTs have been used previously in many studies as reinforcement material in HA powders/scaffolds and as well as in HA coatings applied on titanium-based alloys [3, 9]. Carbon nanotubes are found to increase the fracture toughness, hardness, strength and elastic modulus of HA scaffolds and coatings [9]. Kealley et al. [21] investigated the development of carbon nanotube-reinforced hydroxyapatite bioceramics. Results revealed that the hot iso-statically pressed HA samples showed excellent densification in the presence of 2 wt% CNT and addition of the CNTs had no effect on the structural parameters of the HA phase. Similarly, Meng et al. [22] have reported the formation of a thick apatite layer on 3 wt% CNT-containing HA surfaces prepared by hot pressing after immersion in simulated body fluid for 17 days.

More recently graphene-based materials generally in the form of pristine graphene, graphene oxide and reduced graphene oxide were combined with HA to improve both mechanical properties and cellular adhesion [23, 24]. Liu et al., [24] showed that addition of graphene nanosheets into HA could be an option to improve the biological properties of HA and significantly increased strength has been shown for HA–graphene composites. Previous study of Zeng et al. [23] reported that the addition of graphene oxide to HA coatings have enhanced the crystallinity of deposited apatite particles. Moreover, in vitro cell culture experiments revealed better biocompatibility of composite coatings than the neat HA coating.

Although there are studies in literature on MWCNTs/HA and graphene (generally in the form of graphene oxide and reduced graphene oxide)/HA composites, most of them include preparation of HA-based composites in the form of powders or in the form of coatings over metallic surfaces. Additionally, few studies are present comparing the effects of these two carbon nanostructures on the properties of HA scaffolds. Therefore, in this study, it was intended to prepare porous HA scaffolds with improved mechanical and biological properties to use in bone tissue engineering applications. For this purpose, PCL coating was applied to the surface of HA scaffolds in the presence of graphene nanoflakes and MWCNTs at different concentrations. Microstructure, compression strength, acellular bioactivity and cytotoxicity of the prepared composite scaffolds were investigated and results were discussed.

2 Experimental study

2.1 Scaffold preparation

Commercially available hydroxyapatite (HA), (Trans-Tech, Adamstown, MD) powders were utilized in the study. Particle size distribution of the as-received powders was obtained using a particle size analyzer (Malvern, MasterSizer 3000, UK). Porous, hydroxyapatite scaffolds were prepared using a polymer foam replication technique. For the preparation of the HA suspensions (at 40, 50 and 55 vol%), deionized water was utilized as the solvent. Surface active agents namely Easysphere (Air Products, USA) and Surfynol 104 (Air Products, USA) were used as the dispersant and wetting agent, respectively. Polyvinyl alcohol (Sigma Aldrich, USA) was utilized as the binder in the suspension. The HA slurries were mixed for 3 h using a magnetic stirrer to achieve homogenization. Polyurethane foams (cube-shaped) were immersed into this suspension for 10 min to coat them and squeezed manually to remove the excess HA suspension. The coated foams were dried for 24 h at room temperature and subjected to a heat treatment to decompose the foam and sinter the HA scaffolds. Typically the heating rate was 0.1 °C/min in the range 100–400 °C. Following binder burnout, the constructs were sintered in air atmosphere for 3 h at 1200 °C, using a heating rate of 5°C/min.

The PCL solution at 5 wt% was prepared by dissolving appropriate amount of PCL pellets in anhydrous acetone (Sigma-Aldrich, USA) by stirring at 50 °C for 2 h. Graphene nanopowders in the form of flakes (Graphene Laboratories Inc. USA, Grade AO-4, Average flake thickness: 60 nm, particle (lateral) size :3–7 μm) or multi-walled carbon nanotubes, MWCNTs (Graphene Laboratories Inc. USA, Diameter: 50–85 nm and length: 10–15 μm) at 0.25, 0.5, 1 and 3 wt% were then incorporated into the PCL solution at 50 °C and homogenized using a magnetic stirrer for 1 h followed by homogenization using an ultrasonic horn for an additional 15 min. Sintered HA scaffolds (cube-shape, length: ~ 10 mm) were coated with polycaprolactone solution in the presence of graphene nanoflakes or MWCNTs using dip coating method. Coated scaffolds were dried at room temperature for 48 h prior to characterizations.

2.2 Characterizations

2.2.1 Morphology and mechanical properties

The microstructure was examined using an optical microscope (Olympus, Japan). Porosity measurements were made based on Archimedes method as follows [25]:

$$\text{Porosity}\,(\%) = \frac{[(W_2 - W_3 - W_s)/\rho e]}{(W_1 - W_3/\rho e] + (W_s)/\rho s)} \times 100$$

where W_1 is the weight of the beaker filled with ethanol, W_2 is beaker weight in the presence of ethanol and scaffold, W_3 is weight of the beaker and ethanol after removing the ethanol-saturated scaffold, ρe is density of ethanol, ρ_s is density of scaffold.

The strengths of the cube-shaped scaffolds (length = ~ 10 mm), were measured using a mechanical testing machine (Shimadzu AG-X, Kyoto, Japan) under compression at a deformation rate of 0.5 mm/min. Four different measurements were made for each group of scaffolds and the results were averaged.

2.2.2 Acellular bioactivity

In vitro acellular bioactivity was investigated in simulated body fluid (SBF) at 37 °C under static conditions. SBF was prepared based on the protocol developed by Kokuba et al. [26]. Ion concentrations found in SBF is given in Table 1. Ion concentrations of human plasma are also shown for comparison purpose. In bioactivity experiments, each sample was immersed in a polyethylene bottle containing SBF solution, and kept for 15 days, in an incubator at 37 °C. After removal from the SBF, the scaffolds were dried at 60 °C, sputter-coated with gold and analyzed using a scanning electron microscope, SEM (Philips XL-30S FEG; Eindhoven, Netherlands). Examinations were made at an accelerating voltage of 10 kV and a working distance of 10 mm.

2.2.3 Cell culture experiments

Biological characterizations were performed using mouse bone marrow mesenchymal stem cells, mBMSCs (Cat. No: 66096-23, Celprogen, USA). Prior to experiments, for sterilization purposes scaffolds were kept in 70% ethanol for overnight and exposed to UV light for 60 min. The cells were cultured in a minimum essential medium DMEM (with low glucose, no glutamine, Thermo Fisher Scientific) containing %10 heat-inactivated fetal bovine serum (FBS, Sigma Aldrich,USA) and 0.02% gentamicin (Sigma-Aldrich, USA). Tested scaffolds (length: 5 mm) were placed into each 24-well plate prior to cell seeding. Scaffolds were seeded with cells by adding mBMSC suspension onto the scaffolds (5×10^4 cells in 100 µL of medium per well). The cell-seeded scaffolds were incubated for 3, 7 and 14 days at 37 °C in an atmosphere containing 5% CO_2.

2.2.3.1 MTT assay The cell viability was determined by MTT (3-(4,5-dimethylthiazol-2-yl)-2,5-diphenyltetrazolium bromide) assay (Sigma-Aldrich, USA). After 3, 7 and 14 days of seeding, 100 mL of MTT solution was added to each well and the cells were incubated for an additional 4 h. Then, the medium was removed and the formed formazan crystals were dissolved by dimethyl sulfoxide, DMSO (Sigma-Aldrich, USA). The quantity of formazan (proportional to the number of viable cells) was measured by recording changes in absorbance at 570 nm using a spectrophotometer (Tecan Infinite 200 PRO, Switzerland). Three replicate samples were tested for each condition.

2.2.3.2 Cell morphology After incubation for 14 days scaffolds were removed from culture medium, rinsed three times with phosphate buffer, and subsequently cells were fixed using 2.5% glutaraldehyde solution (Sigma Aldrich, USA). Then they were immersed in phosphate buffer again at 4 °C and kept for overnight. Scaffolds were dehydrated through a graded series of ethanol (50, 60, 70, 80, 90 and 100%) for 15 min at each concentration followed by a treatment with hexamethyldisilazene (Sigma-Aldrich, USA) for 10 min. After drying at room temperature, they were sputter-coated with gold and the surface of the scaffolds was observed using scanning electron microscope.

2.2.4 Statistical analysis

Statistical analysis was performed using One-way ANOVA followed by post hoc Dunnett's and Tukey's Multiple Comparison Test using GraphPad Prism, USA. $p \leq 0.05$ was considered as statistically significant.

Table 1 Ion concentrations of SBF and human blood plasma [27]

Ions (mmol)	Na^+	K^+	Ca^{2+}	Mg^{2+}	Cl^-	HCO_3^-	HPO_4^{3-}	SO_4^{2-}
Human plasma	142.0	5.0	2.5	1.5	103.0	27.0	1.0	0.5
SBF	142.0	5.0	2.5	1.5	148.8	4.2	1.0	0.5

3 Results and discussion

3.1 Morphology and mechanical properties of the bare HA scaffolds

Figure 1 shows the SEM micrographs of the as-received graphene and MWCNT powders. Accordingly, MWCNTs were in the tubular form of carbon and graphene visualized in flake-like structure. Graphene nanopowders were consist of several layers of graphene sheets (flakes) forming agglomerates. It was attributed to the μ–μ bonding that causes the stacking of the individual graphene sheets. Similarly, agglomerate formation in MWCNTs was observed presumably due to presence of attractive van der Waals forces [28, 29]. The SEM micrograph (Fig. 1a) showed that as-received MWCNTs were cross-linked and rope-like entangled bundles exists. On the other hand, particle size analysis results showed that median diameter of the as-received HA particles were 3.1 μm and it has a bimodal particle size distribution (Fig. 1c).

Figure 2a, b show the optical microscope images of bare HA scaffolds prepared in the study after sintering at 1200 °C. The templating method utilized in the study ensured a highly interconnected macro-channeled porous structure. Pore size of the prepared HA scaffolds were measured to be between 400 and 600 μm. The SEM micrograph (Fig. 2c) shows the grain structure of the prepared scaffolds. Average grain size was measured to ~ 2 μm after sintering at 1200 °C. Previous study of Saiz et al. [30] on the preparation of HA scaffolds revealed no phase change for HA constructs after firing at 1300 °C for 3 h. HA samples having relative densities over 99% (theoretical value), and grain sizes on the order of a micrometer, were obtained after sintering at temperatures ranging between 1150 and 1200 °C. Similarly, recent study of Elbadawi et al. [6] showed that the phase purity in HA scaffolds can be kept by sintering until 1300 °C.

Figure 3 demonstrates the porosity and the mechanical testing results of bare scaffolds prepared at different HA concentrations. Accordingly, porosity of the scaffolds was measured to be 77 ± 17% when the HA particle concentration was 40 vol%. On the other hand, porosity decreased to 66 ±26 % when the HA concentration was 55 vol%. Mechanical

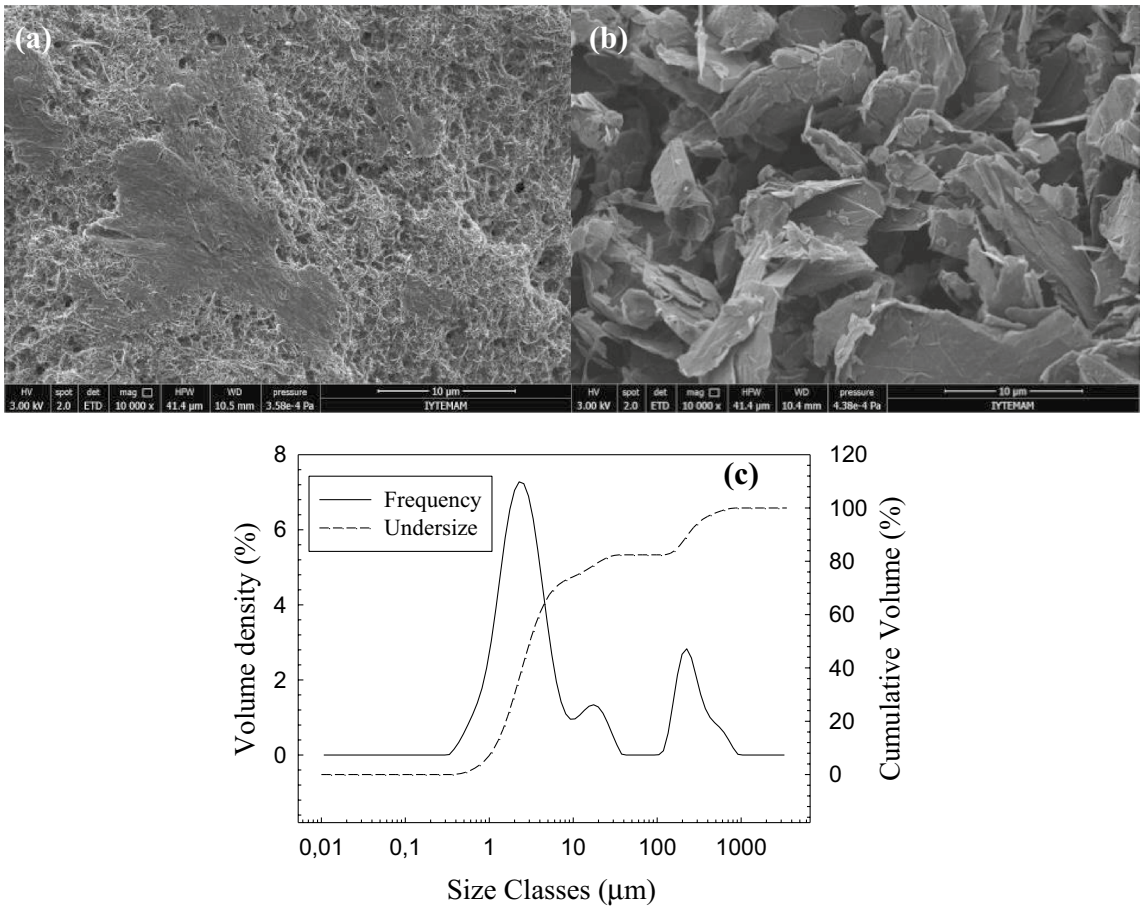

Fig. 1 SEM micrographs of as-received **a** MWCNTs, **b** graphene nanopowders, **c** particle size distribution of HA powders

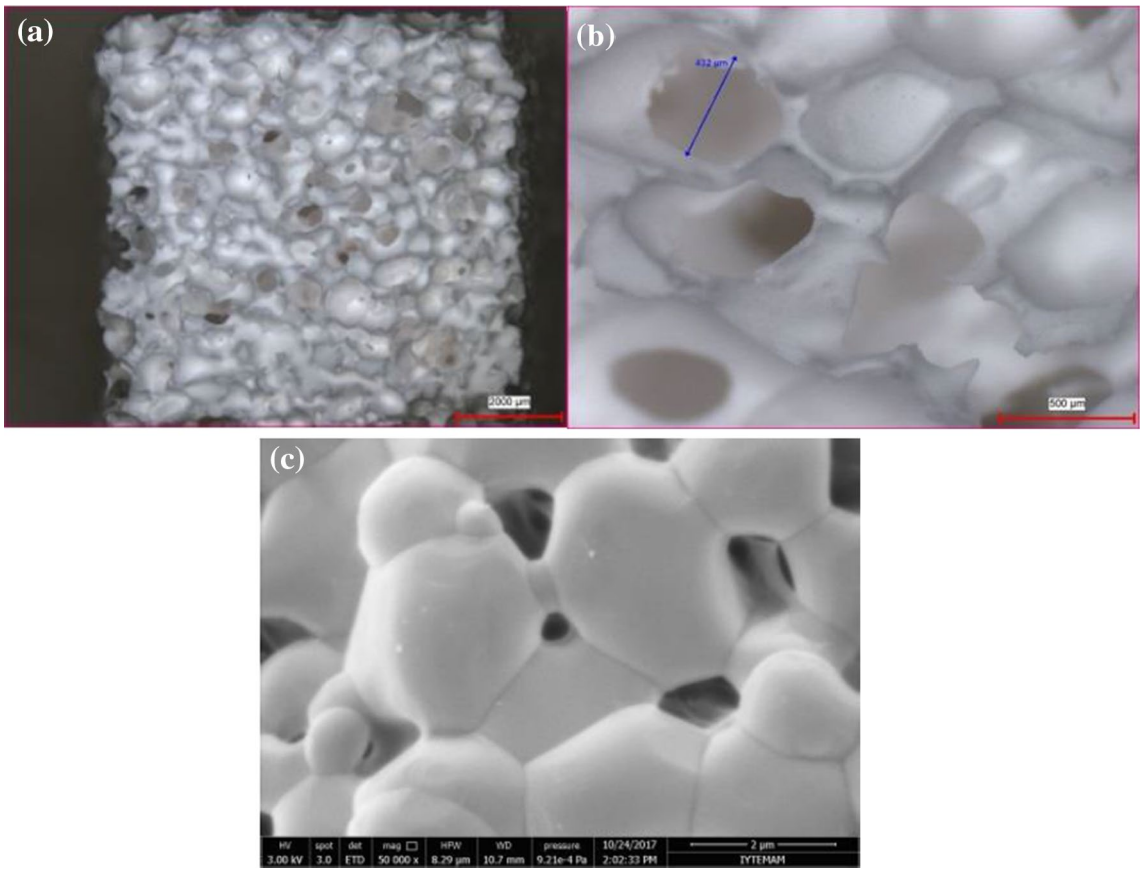

Fig. 2 Optical microscope images **a** low and **b** high magnification and **c** SEM micrograph of HA scaffolds prepared in the study (after sintering at 1200 °C)

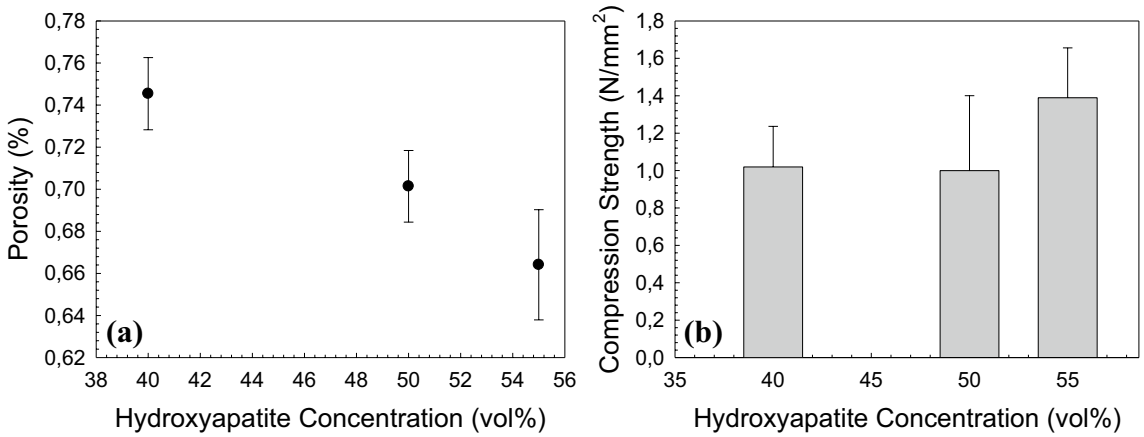

Fig. 3 Graphs showing the **a** porosity and the **b** compression strength of bare HA scaffolds prepared at different concentrations

testing results revealed that the compression strength of the scaffolds prepared at 40 vol% was 1.09 ± 0.21 MPa and it increased to 1.389 ± 0.266 MPa at 55 vol% HA concentration. Based on the high porosity and the moderate compression strength values, it was decided to prepare graphene/MWCNT-containing composite scaffolds using 40 vol% HA. Previously, Gervaso et al. [31] studied on the preparation of HA scaffolds by polymer foam replication technique. Scaffolds (with 90% porosity) had a compressive strength of 0.51 MPa and Weibull modulus was measured to be 4.15.

3.2 Morphology and mechanical properties of composite HA scaffolds

Digital images of graphene and MWCNT-containing PCL-coated HA (40 vol%) scaffolds are given in Fig. 4. Images revealed that all of the prepared scaffolds showed a similar microstructure and they consisted of a network and interconnected cellular pores. PCL coating did not cause any detrimental effect on the pore morphology. Average pore size of the scaffolds was in the range of 100–500 µm. Additionally, graphene nanopowders or MWCNTs were clearly observable inside the HA matrix. Figure 5 demonstrates the higher magnification images of the composite scaffolds containing carbon based additives at different concentrations. Agglomerate formation was more significant in MWCNT-containing samples compared to constructs coated with graphene nanopowders.

Mechanical properties of the prepared composite scaffolds were tested under compression. Figure 6a depicts the strength of the scaffolds as a function of additive concentration. Accordingly, an increase was obtained in compression strength of the PCL-coated HA scaffolds in the presence of graphene and MWCNT at 0.25 wt% and at higher additive concentrations a significant decrease was observed in strength values. Compression strength of the bare HA scaffolds (uncoated) was measured to be 1.09 MPa under the same conditions. By PCL coating (in the absence of additives) strength increased to 2.69 MPa. Previous study of Zhao et al. [12] revealed that the compressive strength of the uncoated highly porous (90%) HA scaffolds prepared by replication method was measured to be 0.09 MPa and it raised to 0.51 MPa by the PCL-coating.

In the current study, highest strength values were obtained for the MWCNT-containing (0.25 wt%) PCL-coated HA scaffolds. Mechanical strength of the prepared composite scaffolds were close to the strength of cancellous bone having 70% porosity [10]. Porosity measurements revealed that addition of graphene or MWCNT to the HA scaffolds in the form of coating reduced the porosity of the constructs (Fig. 6b). A gradual decrease was obtained in porosity of the composite scaffolds as the additive concentration increased. Porosity of the scaffolds containing graphene and MWCNT (at 3 wt%) were measured to be 0.51% and 0.61%, respectively. Stress–strain response of the composite HA based scaffolds in the presence of 0.25 wt% graphene and MWCNT is given in

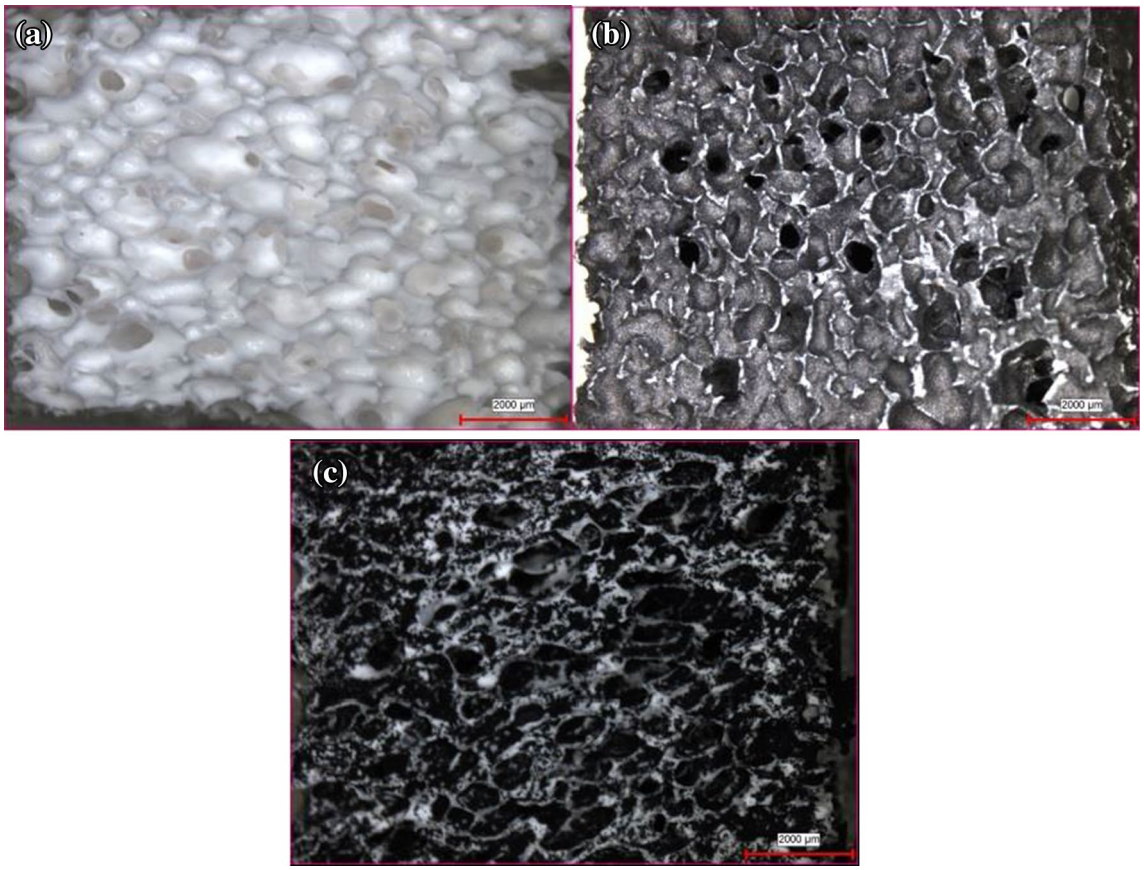

Fig. 4 Optical microscope images of PCL coated composite HA scaffolds **a** bare; **b** 3 wt% graphene; **c** 3 wt% MWCNT; scale bar: 2000 µm

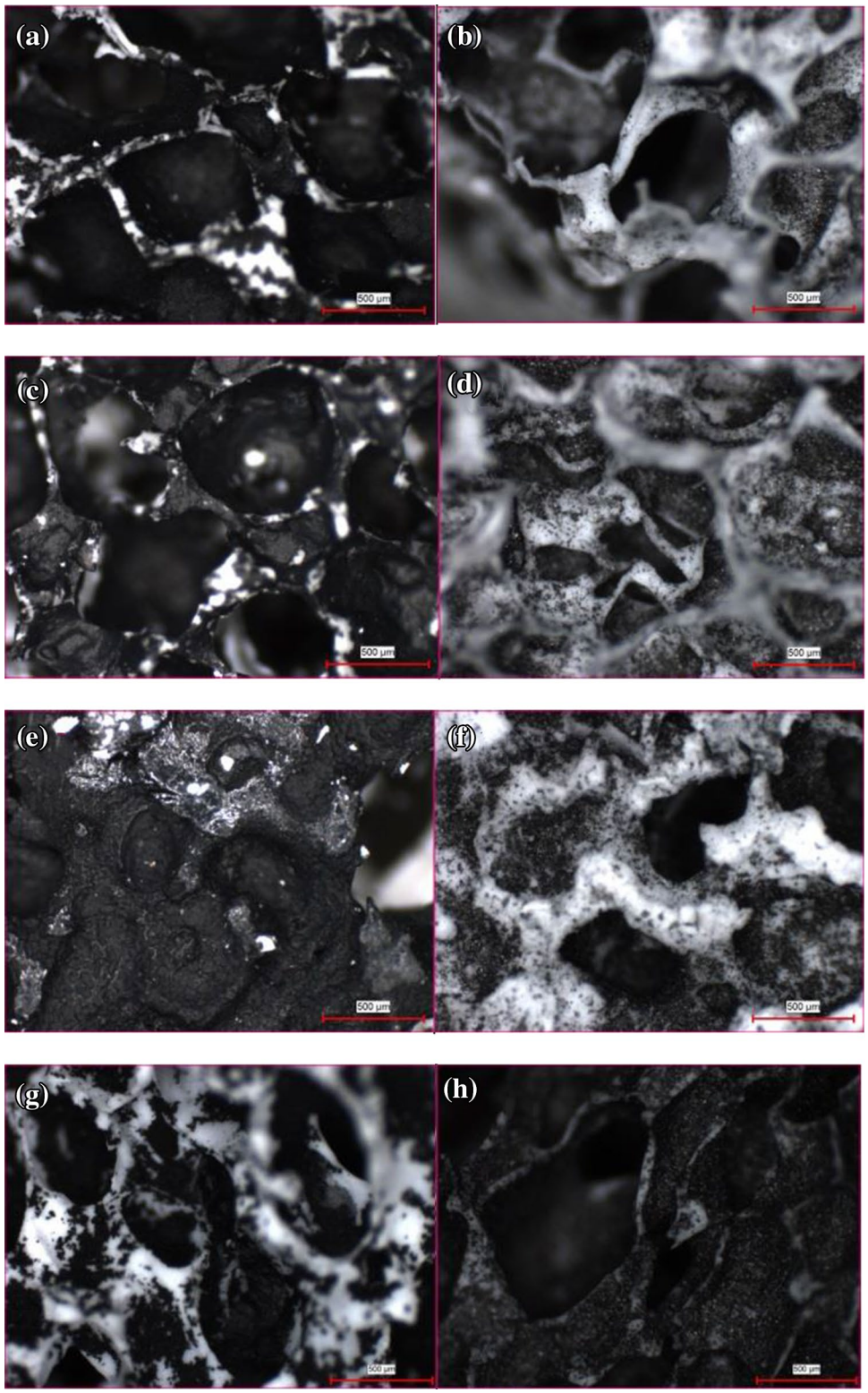

Fig. 5 Optical microscope images of MWCNT (left) and graphene (right)-containing PCL coated scaffolds **a, b** 0.25 wt%; **c, d** 0.5 wt%; **e, f** 1 wt%; **g, h** 3 wt%; scale bar: 500 µm

Fig. 7. Un-coated, bare HA scaffolds showed brittle behavior whereas composite scaffolds showed a typical response of polymer coated ceramic materials with higher strain percentages.

Previouly Touri et al., [32] showed that the incorporation of 0.25 wt% MWCNTs resulted an increase in elastic modulus of 45S5 Bioglass scaffold which was associated with the dispersion of MWCNTs in the matrix serving as a

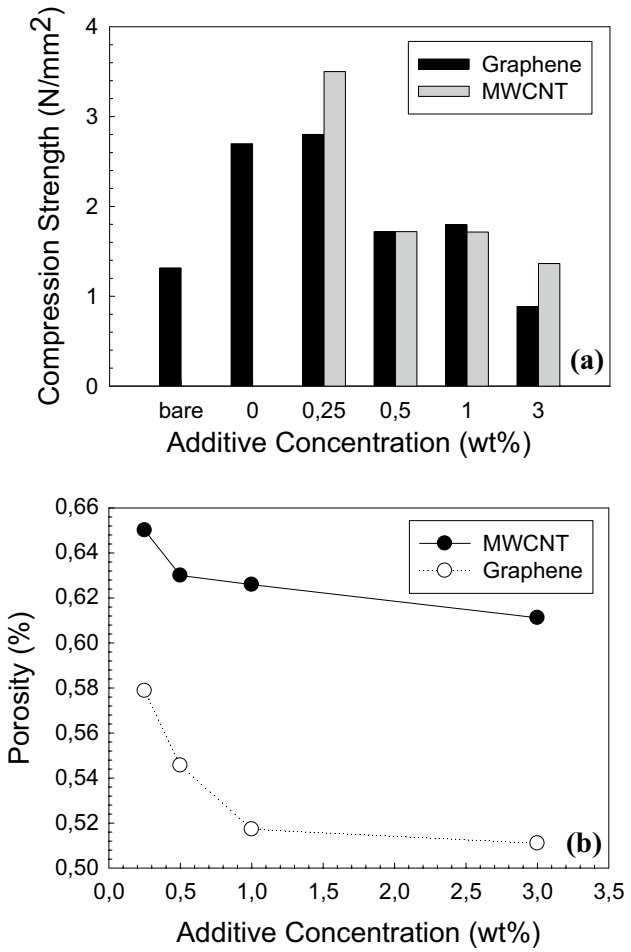

Fig. 6 Graphs showing the **a** compression strength, **b** porosity values of the composite scaffolds prepared in the study (HA 40 vol%)

reinforcing phase. However, when the MWCNT concentration reached to 0.5 wt%, a decrease in the elastic modulus obtained. It was reported that if MWCNT weight fractions are too high, the repulsive forces present on their surface may cause an inhomogeneous dispersion of composite materials and this may leads to a significant decrease of elastic modulus and it may also increase the fragility of the structure. Similarly, in the current study the decrease obtained in compression strength at high additive concentrations may be attributed to the coagulation and inhomogeneous distribution of graphene and MWCNT inside the PCL matrix. The improvement of the compression strength at 0.25% additive concentration can be attributed to the higher elastic modulus of graphene (0.1-1TPa) [33] and MWCNTs (0.2–1 TPa) [34] compared to pure HA. Graphene nanoparticles and MWCNTs have the ability to absorb more stress than HA, resulting in enhanced compression strength of the HA based composites.

3.3 In vitro mineralization

In the study, in vitro mineralization ability of the prepared scaffolds was tested in SBF. Figure 8 show the SEM micrographs of the scaffolds after immersion in SBF for 15 days. The apatite precipitation capability of a scaffold immersed in SBF is an indicator of the in vivo integration ability with the bone tissue [26]. HA is well known for its bioactivity however, the formation of bone apatite on fully sintered HA scaffolds have been hardly detectable [35]. Relatively low sintering temperature is required in retaining OH^- ions and bioactivity [36].

In the study, the surface of the MWCNT-containing (at 3 wt%) PCL-coated HA scaffolds exhibited formation of a plate-like shape material after immersion in SBF. These types of plate-like structures with sharp edges and well-crystallized morphologies are typical of calcium phosphate minerals [37]. At lower MWCNT concentrations formation of a calcium phosphate based material with globular-like morphology was observed. Similarly, in the presence of graphene nanopowders, precipitates of round shape, globular-like HA nano crystals were obtained on the surface of SBF-treated HA composite scaffolds. At lower graphene concentrations and as well as in bare HA scaffolds formation of a calcium phosphate based precipitates were not seen after immersion in SBF for 15 days. This is presumably due to the reduced in vitro mineralization ability of bare HA scaffolds after sintering at 1200 °C for 3 h or requirement of using more saturated SBF solution in bioactivity experiments.

Previous studies have proven that the graphene composite surfaces are suitable for bone-like apatite precipitation and the addition of graphene-based nanofillers into HA matrix could accelerate the formation of apatite on its surface [4, 38]. Ren et al. [39] studied on the bio-mineralization of graphene films by soaking in simulated body fluid. They reported that the graphene films exhibited enhanced mineralization ability in terms of mineral deposition. It was attributed to the high roughness of the graphene films possibily providing more HA nucleation sites. Previous study of Zhang et al. [40] showed that 1 wt% graphene nanosheet/HA composites showed higher apatite mineralization ability compared to pure HA in SBF after 7 days. It was hypothesized that graphene nanosheets create more nucleation sites facilitating apatite mineralization. Meng et al. [41] fabricated 3 wt% CNT-containing HA constructs using hot pressing. Apatite growth rate of the samples immersed in SBF (for 3, 10 and 17 days) was lower in first few days and afterwards became higher. The composites prepared in the study claimed to have high bioactivity [41].

In the previous study of Akasaka et al. [42] MWCNTs were immersed for 2 weeks in the phosphate buffer saline and revised simulated body fluid. SEM observations showed the formation of clusters of spherules consisting

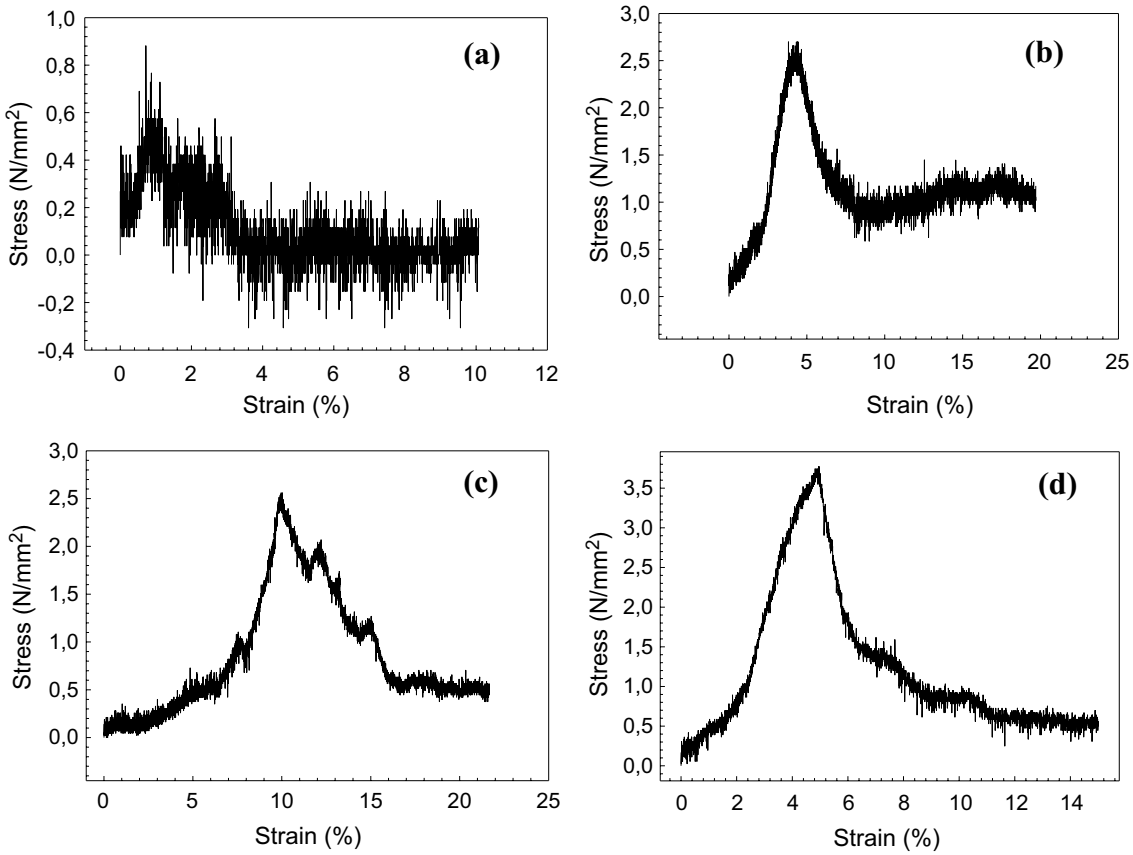

Fig. 7 Stress–strain graphs for **a** bare HA, **b** PCL coated HA, **c** 0.25 wt% graphene, **d** 0.25% MWCNT-containing PCL coated HA scaffolds

of needle-shaped apatite crystallites on the MWCNTs surface. On the other hand, the immersion of MWCNTs in standard SBF showed no apatite formation after 2 weeks.

In the current study, HA formation ability was more pronounced with MWCNTs compared to graphene nanopowders where these additives were possibly acted as an effective nucleation sites to induce the formation of a biomimetic apatite. Another reason for the higher apatite precipitation on composite HA scaffolds may be attributed to the surface charge of the prepared constructs. It is known that the negatively-charged surface enhances the growth of biomimetic CaP and bones rather than the positively-charged surfaces. Stoichiometric HA (Ca/P ratio 1.67) powder suspensions with 5–50 μm has been shown to have a negative charge though zeta potential measurements [43]. Therefore, presence of surface charges on HA bioceramics has shown a significant effect on the crystallization of biological apatite in physiological fluids. Accordingly, graphene/HA and MWCNT/HA composites immersed into SBF is expected to have higher negative charge than pure HA. This may be a possible reason for the faster formation of apatite on their surface.

3.4 Biocompatibility

Biocompatibility of the prepared scaffolds were investigated using bone marrow mesenchymal stem cells (also known as bone marrow-derived mesenchymal stem cells) since they contain a subset of multipotent cells with the potential to repair hard-tissue defects [44]. They are hierarchical postnatal stem/progenitor cells capable of self-renewing and differentiating into osteoblasts, chondrocytes, adipocytes, and neural cells [45].Their capacity to form bone in vivo makes them crucial in regenerative medicine. In the study, mBMSC response to the prepared biocomposite scaffolds was analyzed using MTT assay. Results demonstrating the cell viability rates as a function of additive content and culture time are given in Fig. 9. Accordingly, an increase was obtained in absorbance values indicating the cell viability for graphene/MWCNT-containing scaffolds compared to neat PCL-coated HA constructs. The observed increase in cell viabilities was high especially for scaffolds containing additives at high concentrations. Enhancement in cell viability was significant at 3 wt% concentration for the graphene-containing samples. On the other hand, for the MWCNT-containing samples the

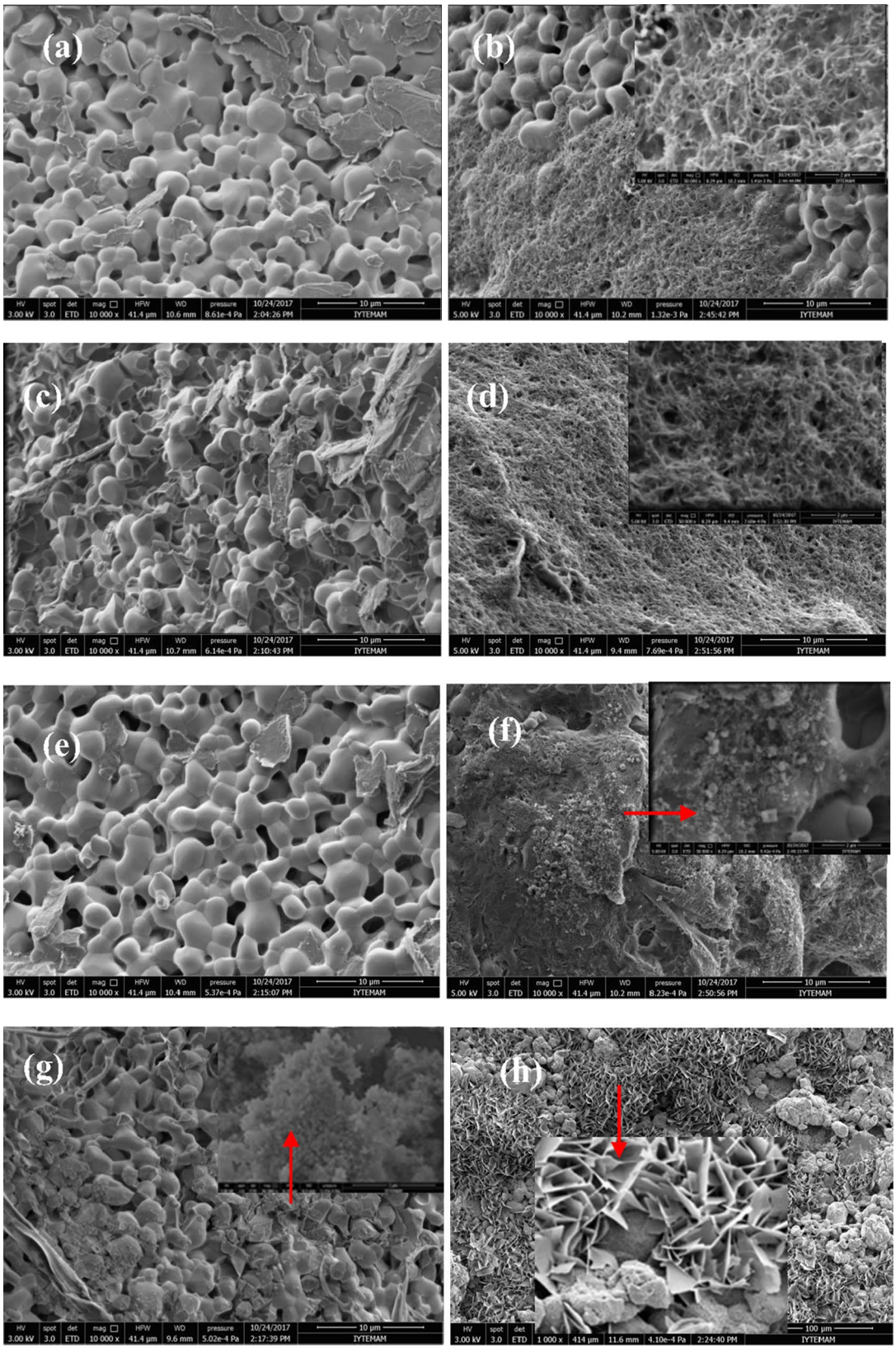

Fig. 8 SEM micrographs of graphene (left) and MWCNT (right)- containing composite HA scaffolds after immersion in SBF for 15 days. **a, b** 0.25 wt%; **c, d** 0.5 wt%; **e, f** 1 wt%; **g, h** 3 wt%; scale bar: 10 µm

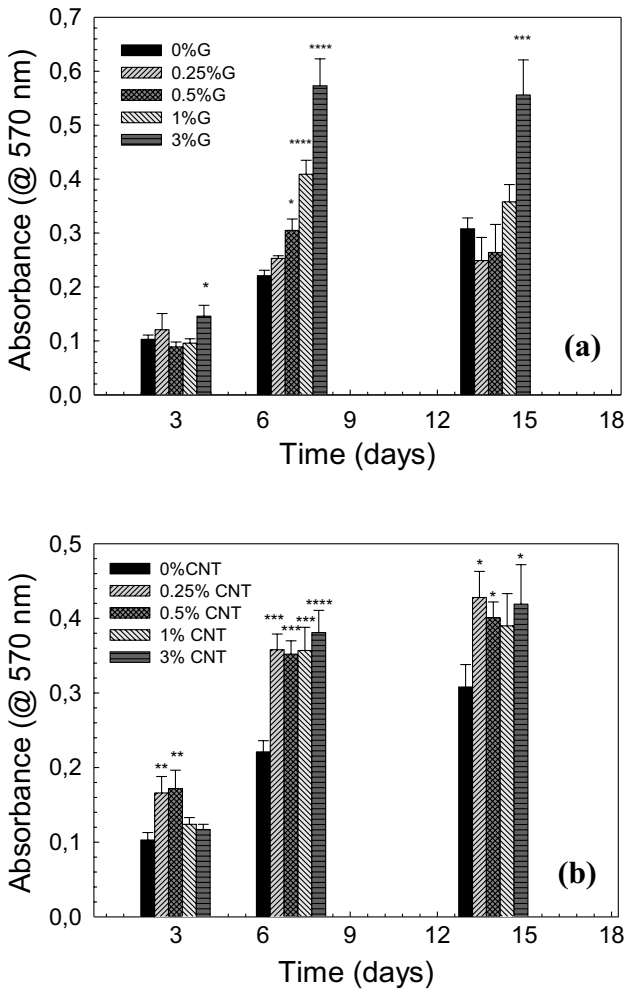

Fig. 9 Graphs showing the MTT assay results for **a** graphene, **b** MWCNT-containing HA scaffolds; $*p \leq 0.05$; $**p \leq 0.01$; $***p \leq 0.001$; $****p \leq 0.0001$

observed increase was significant starting from the lowest additive concentration (0.25 wt%).

In the study cell attachment to the surface of the prepared scaffolds were also investigated. Figure 10 shows the SEM micrographs of the cell seeded scaffolds at 14 days culture time. Accordingly, mBMSCs attached to the surface of the prepared composite scaffolds and they spread on HA–MWCNT and HA- graphene surface with several filopodia protrusions. Additionally, mineralization of extra cellular matrix was clearly observed from the micrographs presumably indicating the osteogenic differentiation of the mBMSCs.

Previous related studies in literature generally report the use of graphene oxide or reduced graphene oxide due to their surface functional groups instead of pristine graphene to prepare composites with HA for biomedical applications. Fan et al. [46] investigated the growth of MC3T3-E1 cells seeded onto graphene nanosheet/HA composites. The synthesized graphene/HA nanorod composite containing 40 wt% HA showed higher osteointegration with surrounding tissues and better biocompatibility than pristine graphene oxide and HA. Liu et al. [47] studied the cytotoxicity of reduced graphene oxide/HA on L929 cells using MTT assay and results showed that the cell viability was more than 95% in comparison with the control group samples. Similarly, Liang et al. [48] have observed increasing viability of fibroblasts on CNT/HA surface up to 100% within 4 days. Results revealed that the osteoblasts attach better on HA surface in the presence of carbon nanotubes [48]. Previous studies have also reported the increase in proliferation as well as the adhesion of osteoblasts on carbon nanotube and graphene surfaces. This may be attributed to the selective absorption and attachment of proteins from cell culture medium by means of carbon\carbon bonds [9, 49]. It is known that carbon nanotubes have high binding affinity to biological molecules such as extracellular matrix proteins. Previously, human mesenchymal stem cells showed improved proliferation and osteogenic differentiation on topologically modified carbon nanotube substrates [50]. Additionally, graphene-based materials allowed stem cell attachment and growth also enhanced the osteogenic differentiation. It was found that although cell proliferation is not improved by pristine graphene, it enhances stem cell differentiation towards osteoblastic lineage [13].

The enhancement of cell attachment and proliferation of bone marrow mesenchymal stem cells observed in the current study may also be attributed to the increased surface roughness due to incorporation of MWCNTs and graphene nanoflakes as well as to the increase in electrical conductivities of the prepared of the scaffolds. It is also important to note that both CNTs and graphene may have cytotoxic effect mainly when they are suspended in fluid medium [13], while they appear nontoxic if immobilized to a matrix such as PCL.

Previously, Torres et al. [51] hypothesized that adding mBMSC concentrate to the hydroxyapatite scaffolds and then placing them in the fracture site would be beneficial for the surgical fixation of hip fractures. Results of their study showed that mBMSCs added to a hydroxyapatite scaffold result in better outcomes after surgical treatment of intertrochanteric hip fractures. Simlarly Mankani et al. [52] showed that when human bone marrow stem cells are transplanted for the purpose of rejeneration of new bone, best results would be achieved if the cells are combined with hydroxyapatite/tricalcium phosphate based materials.

In the current study, it was found that addition of graphene nanoflakes or MWCNTs at specified concentrations may further enhance these outcomes observed previously.

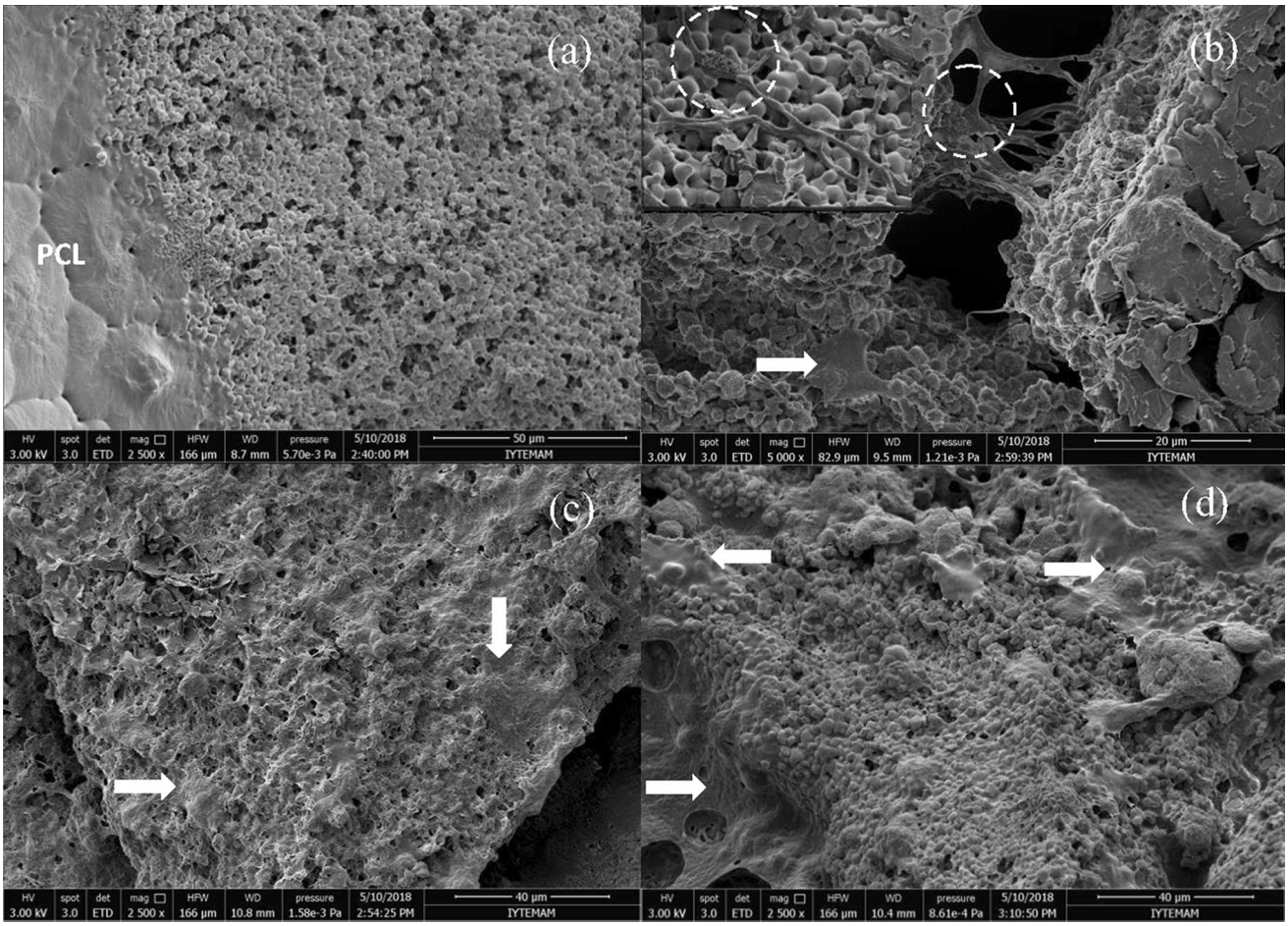

Fig. 10 SEM micrographs showing the cell attachment to the **a** neat and **b, c** graphene, (3 wt%) and **d** MWCNTs (3 wt%)—containing composite scaffolds prepared in the study after 14 days of culture. Arrows indicating cells, dashed area indicating mineralized regions

4 Conclusions

Sponge-like hydroxyapatite scaffolds were manufactured by polymer foam replication method. Graphene nanoflakes and MWCNTs were employed as nanoscale reinforcement agents in hydroxyapatite scaffolds. Surface of the HA scaffolds were coated with PCL in the presence of graphene nanoflakes or MWCNTs. An increase was observed in compression strength of the scaffolds in the presence of 0.25 wt% graphene or MWCNT. Additionally, results revealed that graphene and MWCNTs facilitated the deposition of apatite on the surface of composite HA scaffolds. MTT assay results revealed an increase in mBMSCs viability rates as well as in proliferation for graphene and MWCNT-incorporated HA scaffolds. It was concluded that the addition of an electrically conducting material such as graphene or MWCNTs can enhance the possible applications of HA such as the preparation of electrically conducting HA scaffolds with enhanced mechanical properties and higher bioactivity for the electrically stimulated growth of the cells. The in vivo investigation to predict the suitability of mBMSC seeded, graphene/MWCNT-containing PCL-coated HA composite scaffolds for orthopedic applications will be the goal of future study.

Acknowledgements The financial support for this research was provided by the Scientific and Technical Research Council of Turkey (TÜBİTAK), Grant No: 114M519.

References

1. B. Ben-Nissan, Curr. Opin. Solid State Mater. Sci. **7**(4–5), 283–288 (2003)
2. D. Milovac, G.G. Ferrer, M. Ivankovic, H. Ivankovic, Mater. Sci. Eng. C **34**, 437–445 (2014)
3. K. Balani, R. Anderson, T. Laha, M. Andara, J. Tercero, E. Crumpler, A. Agarwal, Biomaterials **28**(4), 618–624 (2007)
4. W.J. Basirun, B. Nasiri-Tabrizi, S. Baradaran, Crit. Rev. Solid State Mater. Sci. **43**, 1–36 (2017)
5. M. Li, Q. Liu, Z. Jia, X. Xu, Y. Cheng, Y. Zheng, T. Xi, S. Wei, Carbon **67**, 185–197 (2014)

6. M. Elbadawi, J. Meredith, M. Mosalagae, I.M. Reaney, Adv. Mater. Lett. **8**(4), 377–385 (2017)
7. S.V. Dorozhkin, Biomaterials **31**(7), 1465–1485 (2010)
8. Y. Liu, J. Huang, M. Niinomi, H. Li, Ceram. Int. **42**, 11248–11255 (2016)
9. D. Lahiri, S. Ghosh, A. Agarwal, Mater. Sci. Eng. C **32**, 1727–1758 (2012)
10. R. Havaldar, S.C. Pilli, B.B. Putti, Adv. Biomed. Res. **3**, 101 (2014)
11. B.D. Ulery, L.S. Nair, C.T. Laurencin, J. Polym. Sci. B **49**, 832–864 (2011)
12. J. Zhao, K. Duan, J.W. Zhang, X. Lu, J. Weng, Appl. Surf. Sci. **256**, 4586–4590 (2010)
13. N. Dubey, R. Bentini, I. Islam, T. Cao, A.H. Castro Neto, V. Rosa, Stem Cells Int. **2015**, 12 (2015)
14. N. Saifuddin, A.Z. Raziah, A.R. Junizah, J. Chem. **2013**, 18 (2013)
15. M. Naebe, J. Wang, A. Amini, H. Khayyam, N. Hameed, L.H. Li, Y. Chen, B. Fox, Nat. Sci. Rep. **4**, 4375 (2014)
16. S. Stankovich, D.A. Dikin, G.H. Dommett, K.M. Kohlhaas, E.J. Zimney, E.A. Stach, R.D. Piner, S.T. Nguyen, R.S. Ruoff, Nature **442**, 282–286 (2006)
17. L.S. Walker, V.R. Marotto, M.A. Rafiee, N. Koratkar, E.L. Corral, ACS Nano **5**(4), 3182–3190 (2011)
18. S. Kim, S.H. Ku, S.Y. Lim, J.H. Kim, C.B. Park, Adv. Mater. **23**, 2009–2014 (2011)
19. C. Gao, T. Liu, C. Shuai, S. Peng, Sci. Rep. **4**, 4712 (2014)
20. H. Shen, L. Zhang, M. Liu, Z. Zhang, Theranostics **2**(3), 283–294 (2012)
21. C. Kealley, M. Elcombe, A. van Riessen, B. Ben-Nissan, Physica B **385–386**, 496–498 (2006)
22. Y.H. Meng, C.Y. Tang, C.P. Tsui, D.Z. Chen, J. Mater. Sci.: Mater. Med. **19**(1), 75–81 (2008)
23. Y. Zeng, X. Pei, S. Yang, H. Qin, H. Cai, S. Hu, L. Sui, Q. Wan, J. Wan, Surf. Coat. Technol. **286**, 72–79 (2016)
24. Y. Liu, J. Huang, H. Li, J. Mater. Chem. B. **1**, 1826–1834 (2013)
25. M.-J. Chern, L.-Y. Yang, Y.-K. Shen, J.-H. Hung, Int. J. Precis. Eng. Manuf. **14**, 2201–2207 (2013)
26. T. Kokubo, H. Kushitani, S. Saka, T. Kitsugi, T. Yamamuro, J. Biomed. Mater. Res. **24**, 721–734 (1990)
27. N. Nezafati, F. Moztarzadeh, S. Hesaraki, Biotechnol. Bioprocess. Eng. **17**(4), 746–754 (2012)
28. J. Ervina, M. Mariatti, S. Hamdan, Procedia Chem. **19**, 897–905 (2016)
29. R. Atif, F. Inam, Beilstein J. Nanotechnol. **7**, 1174–1196 (2016)
30. E. Saiz, L. Gremillard, G. Menendez, P. Miranda, K. Gryn, A.P. Tomsia, Mater. Sci. Eng. C **27**, 546–550 (2007)
31. F. Gervaso, F. Scalera, S.K. Padmanabhan, A. Sannino, A. Licciulli, Int. J. Appl. Ceram. Technol. **9**(3), 507–516 (2012)
32. R. Touri, F. Moztarzadeh, Z. Sadeghian, D. Bizari, M. Tahriri, M. Mozafari, Biomed. Res. Int. **2013**, 8 (2013)
33. S. Ryu, B.S. Kim, Tissue Eng. Regen. Med. **10**(2), 39–46 (2013)
34. F. Luo, L. Pan, X. Pei, R. He, J. Wang, Q. Wan, in *Handbook of Polymer Nanocomposites: Processing, Performance and Application*, ed. by K. Kar, J. Pandey, S. Rana (Springer, Berlin, 2015), pp. 173–193
35. D. L.Kaewsichan, P. Riyapan, J. Prommajan, Kaewsrichan, Sci. Asia **37**, 240–246 (2011)
36. M. Prakasam, J. Locs, K. Salma-Ancane, D. Loca, A. Largeteau, L. Berzina-Cimdina, J. Funct. Biomater. **6**, 1099–1140 (2015)
37. A. Polini, J. Wang, H. Bai, Y. Zhu, A.P. Tomsia, C. Mao, Biomater. Sci. **2**, 1779–1786 (2014)
38. M. Li, P. Xiong, F. Yan, S. Li, C. Ren, Z. Yin, A. Li, H. Li, X. Ji, Y. Zheng, Y. Cheng, Bioact. Mater. **3**(1), 1–18 (2018)
39. J. Ren, X. Zhang, Y. Chen, Carbon Lett. **22**, 42–47 (2017)
40. L. Zhang, W. Liu, C. Yue, T. Zhang, P. Li, Z. Xing, Y. Chen, Carbon **61**, 105–115 (2013)
41. Y.H. Meng, C.Y. Tang, C.P. Tsui, Mater. Sci. Forum **532–533**, 201–204 (2006)
42. T. Akasaka, F. Watari, Y. Sato, K. Tohji, Mater. Sci. Eng. C **26**(4), 675–678 (2006)
43. J. Vandiver, D. Dean, N. Patel, W. Bonfield, C. Ortiz, Biomaterials **26**, 271–283 (2005)
44. S. Liu, L.F. de Castro, P. Jin, S. Civini, J. Ren, J.A. Reems, J. Cancelas, R. Nayak, G. Shaw, T. O'Brien, D.H. McKenna, M. Armant, L. Silberstein, A.P. Gee, D.J. Hei, P. Hematti, S.A. Kuznetsov, P.G. Robey, D.F. Stroncek, Sci. Rep. **7**, 46731 (2017)
45. K. Akiyama, Y.-O. You, T. Yamaza, C. Chen, L. Tang, Y. Jin, X-D. Chen, S. Gronthos, S. Shi, Stem Cell Res. Ther. **3**, 40 (2012)
46. Z. Fan, J. Wang, Z. Wang, H. Ran, Y. Li, L. Niu, P. Gong, B. Liu, S. Yang, Carbon **66**, 407–416 (2014)
47. H. Liu, P. Xi, G. Xie, Y. Shi, F. Hou, L. Huang, F. Chen, Z. Zeng, C. Shao, J. Wang, J. Phys. Chem. C **116**, 3334–3341 (2012)
48. C. Liang, H. Li, L. Wang, X. Chen, W. Zhao, Mater. Chem. Phys. **124**, 21–24 (2010)
49. M. Matsuoka, T. Akasaka, Y. Totsuka, F. Watari, Mater. Sci. Eng. B **173**, 182–186 (2010)
50. J.-R. Lee, S. Ryu, S. Kim, B.-S. Kim, Biomater Res. **19**, 3 (2015)
51. J. Torres, M. Gutierres, M. Ascenção Lopes, J. Domingos Santos, A.T. Cabral, R. Pinto, C. van Eck, Biomed. Res. Int. **2014**, 451781 (2014)
52. M.H. Mankani, S.A. Kuznetsov, R.M. Wolfe, G.W. Marshall, P.G. Robey, Stem Cells **24**(9), 2140–2149 (2006)